Correction

MEDICAL SCIENCES

Correction for "Identification of hydroxyapatite spherules provides new insight into subretinal pigment epithelial deposit formation in the aging eye," by Richard B. Thompson, Valentina Reffatto, Jacob G. Bundy, Elod Kortvely, Jane M. Flinn, Antonio Lanzirotti, Emrys A. Jones, David S. McPhail, Sarah Fearn, Karsten Boldt, Marius Ueffing, Savanjeet Guy Singh Ratu, Laurenz Pauleikhoff, Alan C. Bird, and Imre Lengyel, which appeared in issue 5, February 3, 2015, of *Proc Natl Acad Sci USA* (112:1565–1570; first published January 20, 2015; 10.1073/pnas.1413347112).

The authors note that reference 16 appeared incorrectly. The corrected reference appears below.

16. Johnson LV, et al. (2002) The Alzheimer's Aβ-peptide is deposited at sites of complement activation in pathologic deposits associated with aging and age-related macular degeneration. *Proc Natl Acad Sci USA* 99(18):11830–11835.

www.pnas.org/cgi/doi/10.1073/pnas.1511664112

CORRECTION

Identification of hydroxyapatite spherules provides new insight into subretinal pigment epithelial deposit formation in the aging eye

Richard B. Thompson[a], Valentina Reffatto[b], Jacob G. Bundy[c], Elod Kortvely[d], Jane M. Flinn[e], Antonio Lanzirotti[f], Emrys A. Jones[c], David S. McPhail[g], Sarah Fearn[g], Karsten Boldt[d], Marius Ueffing[d], Savanjeet Guy Singh Ratu[b], Laurenz Pauleikhoff[b], Alan C. Bird[b], and Imre Lengyel[b,1]

[a]Department of Biochemistry and Molecular Biology, University of Maryland School of Medicine, Baltimore, MD 21201; [b]Institute of Ophthalmology, University College London, London EC1Y 8TB, United Kingdom; Departments of [c]Surgery and Cancer and [g]Materials, Imperial College London, South Kensington, London SW7 2AZ, United Kingdom; [d]Centre for Ophthalmology, University of Tübingen, D-72076 Tubingen, Germany; [e]Department of Psychology, George Mason University, Fairfax, VA 22030; and [f]Center for Advanced Radiation Sources, The University of Chicago, Chicago, IL 60439

Edited by Jeremy Nathans, Johns Hopkins University, Baltimore, MD, and approved December 22, 2014 (received for review July 28, 2014)

Accumulation of protein- and lipid-containing deposits external to the retinal pigment epithelium (RPE) is common in the aging eye, and has long been viewed as the hallmark of age-related macular degeneration (AMD). The cause for the accumulation and retention of molecules in the sub-RPE space, however, remains an enigma. Here, we present fluorescence microscopy and X-ray diffraction evidence for the formation of small (0.5–20 μm in diameter), hollow, hydroxyapatite (HAP) spherules in Bruch's membrane in human eyes. These spherules are distinct in form, placement, and staining from the well-known calcification of the elastin layer of the aging Bruch's membrane. Secondary ion mass spectrometry (SIMS) imaging confirmed the presence of calcium phosphate in the spherules and identified cholesterol enrichment in their core. Using HAP-selective fluorescent dyes, we show that all types of sub-RPE deposits in the macula, as well as in the periphery, contain numerous HAP spherules. Immunohistochemical labeling for proteins characteristic of sub-RPE deposits, such as complement factor H, vitronectin, and amyloid beta, revealed that HAP spherules were coated with these proteins. HAP spherules were also found outside the sub-RPE deposits, ready to bind proteins at the RPE/choroid interface. Based on these results, we propose a novel mechanism for the growth, and possibly even the formation, of sub-RPE deposits, namely, that the deposit growth and formation begin with the deposition of insoluble HAP shells around naturally occurring, cholesterol-containing extracellular lipid droplets at the RPE/choroid interface; proteins and lipids then attach to these shells, initiating or supporting the growth of sub-RPE deposits.

hydroxyapatite | age-related macular degeneration | retinal pigment epithelium | drusen | calcium

A major feature of the aging retina is the deposition of proteins (1) and lipids (2) external to the retinal pigment epithelium (RPE), leading to the formation of sub-RPE deposits that can be focal (drusen) or diffuse (basal linear and basal laminar deposits) (3, 4). Sub-RPE deposits increase in number and size with age, and are believed to impair metabolic exchange between the choroidal blood circulation and the retina (5). This blockage of nutrient and waste flow to and from the highly active photoreceptors is widely suspected of inducing degeneration of the sensory retina, particularly in the macula, eventually leading to age-related macular degeneration (AMD). Due to this correlation between AMD and sub-RPE deposit formation, substantial effort has been devoted to determining the composition and origin of sub-RPE deposits, with a view to developing better diagnosis, prevention, and treatment for AMD (4). Although AMD does not necessarily follow the same course in all patients (6), it is acknowledged that progression of sub-RPE deposit formation is a major factor in a large proportion of cases.

There is compelling evidence for the production and secretion of cholesterol-containing lipids and lipoprotein particles, secreted at least partly by the RPE (7, 8), that are recruited and retained in the aging Bruch's membrane (9–14). However, there is no unifying explanation of how and why proteins are recruited and retained at the RPE/choriocapillaris interface. Given the high degree of protein heterogeneity within sub-RPE deposits, it was puzzling why specific proteins, such as amyloid beta or complement factor H (CFH), appear therein as hollow, spherule-like structures (15, 16). Here, we identify numerous hollow hydroxyapatite (HAP) spherules with lipid cores in all examined sub-RPE deposits, with proteins bound to the spherules' surfaces. Individual HAP spherules are also present external to the RPE, and we propose that these HAP spherules are involved in protein deposition at the RPE/choroid interface and contribute to the growth of sub-RPE deposits.

Results and Discussion

As part of our ongoing studies to determine the composition of sub-RPE deposits (17, 18), we collected microfocused synchrotron X-ray diffraction (μXRD) patterns from isolated sub-RPE deposits from human cadaver eyes. The μXRD pattern clearly identified HAP in sub-RPE deposits (Fig. 1 *A* and *B*),

Significance

Proteins and lipids accumulating in deposits external to the retinal pigment epithelium (RPE) represent a barrier to metabolic exchange between the retina and the choroidal capillaries. With time, these deposits can lead to age-related macular degeneration (AMD), the most common cause of blindness in the elderly in the developed world. It remains unclear how sub-RPE deposits are initiated and grow to clinically relevant features. Using a combination of high-resolution analytical techniques, we found that tiny hydroxyapatite (bone mineral) spherules with cholesterol-containing cores are present in all examined sub-RPE deposits, providing a scaffold to which proteins adhere. If the spherules are important in initiating sub-RPE deposit formation, this finding may provide attractive new approaches for early identification and treatment of AMD.

Author contributions: R.B.T., J.G.B., E.K., D.S.M., A.C.B., and I.L. designed research; R.B.T., V.R., E.K., J.M.F., E.A.J., S.F., S.G.S.R., L.P., and I.L. performed research; R.B.T., V.R., J.G.B., E.K., J.M.F., A.L., E.A.J., D.S.M., S.F., K.B., M.U., A.C.B., and I.L. analyzed data; and R.B.T., J.G.B., E.K., D.S.M., A.C.B., and I.L. wrote the paper.

The authors declare no conflict of interest.

This article is a PNAS Direct Submission.

[1]To whom correspondence should be addressed. Email: i.lengyel@ucl.ac.uk.

This article contains supporting information online at www.pnas.org/lookup/suppl/doi:10.1073/pnas.1413347112/-/DCSupplemental.

demonstrating that this highly insoluble form of calcium phosphate [$Ca_5(PO_4)_3OH$, also called hydroxylapatite], which is ordinarily found in bones and teeth, is present in sub-RPE deposits. Ectopic calcification of soft tissues has been associated with the general aging process, and significant calcification of the collagenous layer of Bruch's membrane is typically present in AMD (19). This calcification can be readily labeled with Von Kossa's stain (20), which indicates the presence of calcium phosphates. However, compared with other calcium phosphates, HAP is much less soluble; more stable; mechanically harder; and, to our knowledge, solubilized physiologically only with acid treatment (21). Small internal spherules with calcium content have been noted in sub-RPE deposits before (20, 22), but HAP has not been associated with these spherules.

We imaged HAP in sub-RPE deposits in human cadaver eyes by confocal fluorescence microscopy using four stains that are known to label HAP in bones and teeth. These stains were tetracycline (Sigma–Aldrich) (23) and its analog, Bone-Tag 680 RD (Li-Cor) (24), Alizarin Red S (Sigma–Aldrich) (25), and Xylenol Orange (Sigma–Aldrich) (26). Three of these compounds have differing HAP-binding moieties (Fig. S1), making it unlikely that the very similar fluorescent staining with each compound was due to nonspecific binding to some other molecule(s), such as a protein. These stains are specific for HAP in contrast to dibasic calcium or zinc phosphates (Fig. S2), and they all displayed very similar staining patterns in freshly dissected flat mounts of human cadaver retinas (Fig. S3). Bone-Tag 680 RD fluorescence (depicted in magenta in Fig. 1 *C* and *D* and used in most of the experiments) was present in small (0.5–20 μm in diameter, average size of ∼3 μm) spherules within all sub-RPE deposits. This fluorescence was quite distinct from the typical tissue autofluorescence (27) (depicted in green in Fig. 1 *F*–*H*) or pigment granules. The spherules typically exhibited a hollow appearance, indicating that the dyes did not stain the core of the spherules (Fig. 1 *D*–*H*). This lack of staining was not simply a consequence of poor dye penetration because sectioned specimens with HAP stained on the cut face appeared hollow as well (Movie S1). The number of HAP spherules varied among sub-RPE deposits: There were only a few present in some, and there were dozens present in others (Fig. 1 *D*–*F*). In addition, we identified spherules that were not surrounded by the autofluorescence typical of sub-RPE deposits (27) (Fig. 1 *G* and *H*). Essentially identical spherules were observed in sub-RPE deposits in all 30 eyes from different donors that we received in a 6-mo period, with the donors having an age range of 43–96 y (Table S1). There was a direct relationship between the thickness of the sub-RPE deposits and the number and size of drusen on the one hand and the number of HAP-labeled spherules on the other hand. There were no obvious gender differences in the labeling, although there were variations in retinal location. Some eyes contained large, soft, drusen-like deposits in the macula (Fig. 1*A* and labeled with *** in Table S1), suggesting that these donors had early AMD. Large areas covered by diffuse deposits were reminiscent of basal laminar or linear deposits (Fig. 1*B*). With our current light microscopy approach using unfixed tissues, we were not able to identify the different subtypes of sub-RPE deposits unambiguously. However, all eyes contained hard, drusen-like deposits mainly located at the retinal periphery (Fig. 1 *C* and *D* and labeled with * in Table S1). Spherules were occasionally seen in isolation in the sub-RPE space (Fig. 1 *E* and *F*).

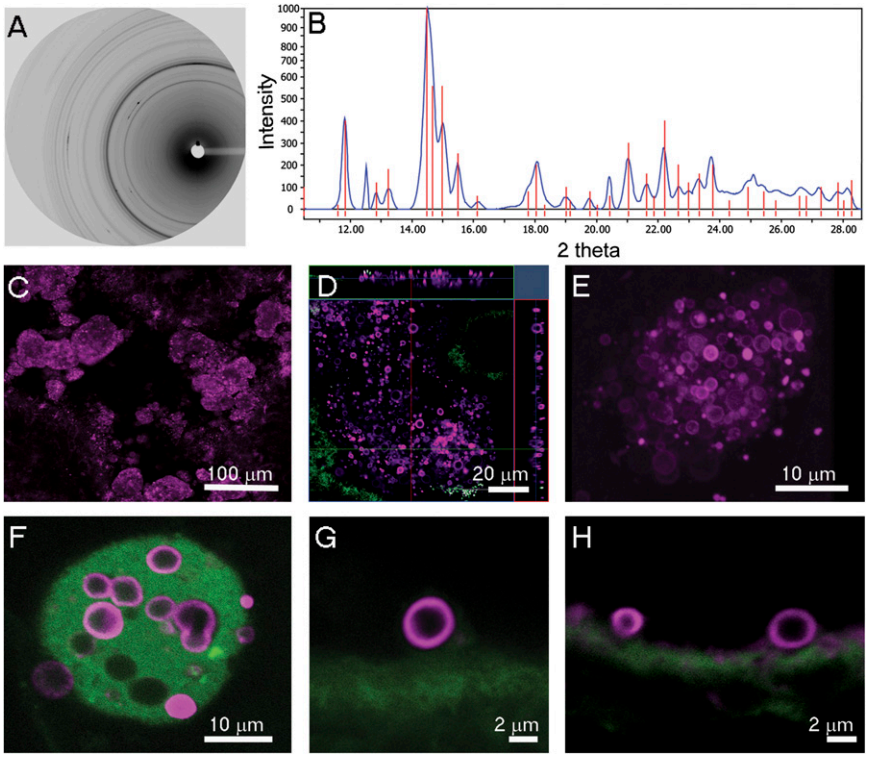

Fig. 1. HAP is present in sub-RPE deposits as spherular structures. The X-ray diffraction pattern (*A*) and radial intensity profile (*B*) confirmed the presence of HAP in isolated sub-RPE deposits. Red lines in *B* indicate the position of diffraction peaks for pure HAP powder. (*C*–*F*) Deposits contain numerous HAP spherules (magenta, stained with Bone-Tag 680RD) in sub-RPE deposits. Optical sectioning using confocal microscopy revealed that HAP forms spherules throughout macular large drusen (*D*) as well as in hard drusen (*E* and *F*), but sperules were also seen in the absence of the typical autofluorescence (green) of sub-RPE deposits and Bruch's membrane (*G* and *H*).

The similarity of form and hollow nature of the spherules raised the question of what may be in the center that promotes the formation of the HAP shell. Lipids are actively transported through Bruch's membrane (2, 10) and can be coated by HAP in vivo (28). Therefore, unfixed whole-mount samples were stained with Nile Red, a fluorescent dye for neutral lipids. Nile Red dye labeled a large number of spherical inclusions with diameters similar to HAP spherules in these samples (Fig. S4). Unfortunately, double labeling with Nile Red and the HAP dyes was unsuccessful due to incompatibilities of the reagents. Therefore, we analyzed the composition of flat-mounted and freeze-dried (Fig. 2*E*) sub-RPE deposits by MS imaging. For this experiment, sub-RPE deposits (a druse in Fig. 2) were "milled" (without fixation or mechanical sectioning) using a focused ion beam (FIB) to reveal the inner structure of the druse (Fig. 2 *A* and *B*) while preserving the native chemical composition. The milled samples were then analyzed with TOF secondary ion mass spectrometry (SIMS), which is well suited to this investigation because it combines high lateral resolution (~250 nm) and high sensitivity (29), and images molecular ions and organic molecules over a wide mass range. A multivariate image analysis (nonnegative matrix factorization score plot) clearly demonstrated chemically distinct spherular structures inside the drusen (Fig. 2*F*). Further analysis of selected ions provided detailed and independent maps of calcium phosphate (Fig. 2*C*); organic molecules, such as cholesterol (Fig. 2*D*); ions characteristic of phosphatidylcholine (PC) (Fig. 2*G*); and overall protein signature (Fig. 2*H*). Neither the readily identified *m/z* 184 ion, derived from phosphocholine headgroups, nor those characteristic of protein signatures showed enrichment in spherules. The ionic signatures for other phospholipids and/or triglycerides were not detected at this spatial resolution. However, the spherules in sub-RPE deposits clearly contain calcium phosphate (these experiments did not distinguish the different calcium phosphates), and they are also associated with cholesterol and/or cholesteryl esters in accord with previous observations on the composition of extracellular lipid droplets in Bruch's membrane and sub-RPE deposits (11, 30).

The shells shown in Fig. 1 are strikingly similar to images previously obtained by immunohistochemical staining of proteins earlier identified as constituents of sub-RPE deposits, such as amyloid beta (15, 16), CFH (31), and vitronectin (32). HAP is

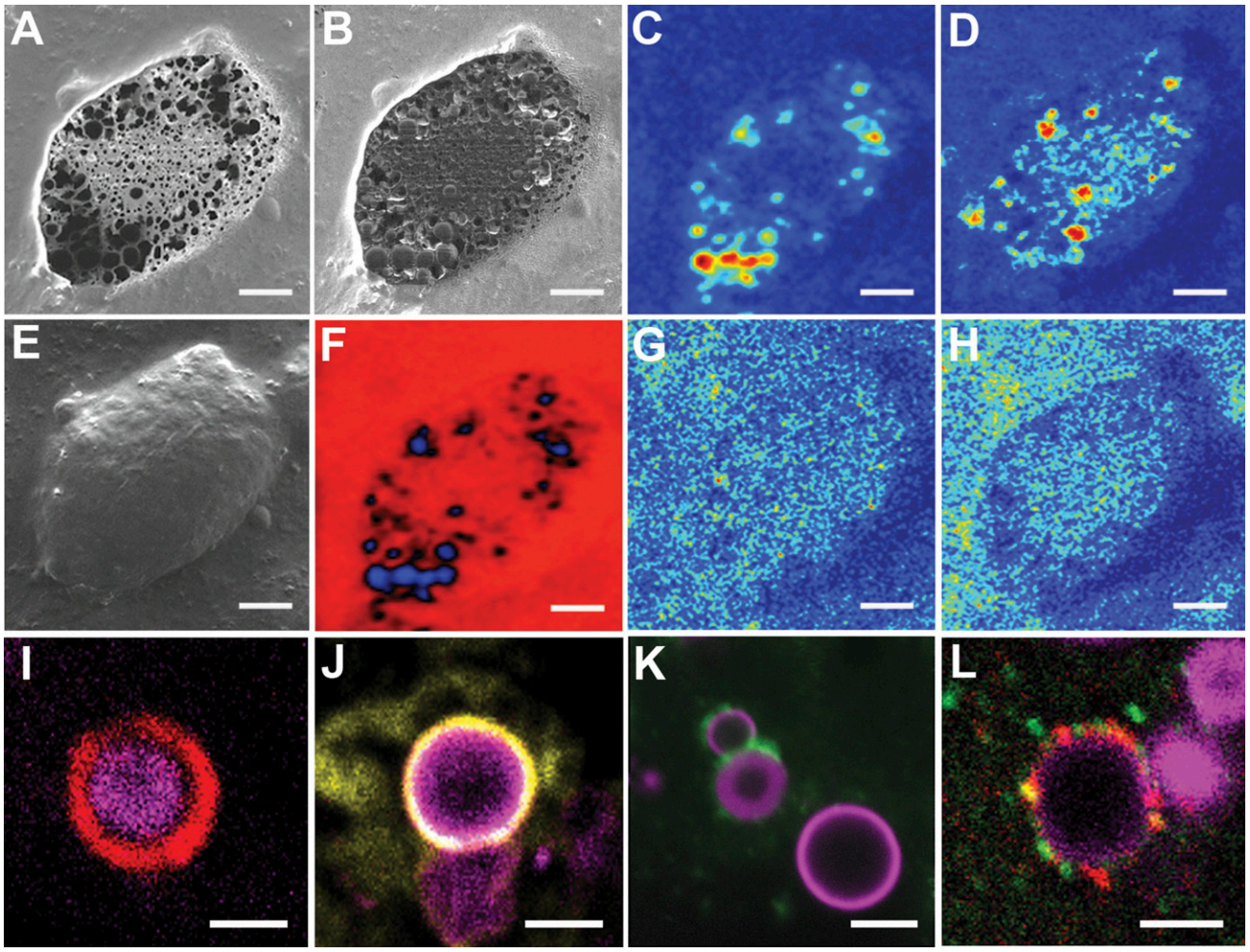

Fig. 2. Identification of molecular constituents of the inner core and outer surface of HAP spherules by TOF-SIMS. Secondary electron (*A*) and secondary ion (*B*) images of the inner structures after FIB milling of a deposit (*E*). (*F*) Nonnegative matrix factorization score plot demonstrates chemically distinct spherules inside the deposit. Positive ion SIMS images confirmed the selective enrichment of calcium phosphate (*C*) and cholesterol (*D*), but not the PC head-group (*G*) or combined signals from protein fragments (*H*) associated with the HAP spherules. Immunohistochemical fluorescent labeling with protein-specific antibodies revealed that HAP spherules (*I–L*, magenta) were found coated with amyloid beta (*I*, red), vitronectin (*J*, yellow), and CFH (*K*, green), or colabeled by a combination of these proteins [*L*, red (amyloid beta) and green (CFH)]. (*L* and *K*) Not all of the spherules are labeled by the antibodies used, indicating diverse protein binding to HAP spherules. (Scale bars: *A–H*, 10 μm; *I–L*, 2 μm.)

well known to bind proteins, and for this reason, it is widely used as a stationary phase for chromatography (33). Consequently, we tested the hypothesis that the HAP spherules promote the growth of the protein-rich sub-RPE deposits by binding proteins present in the sub-RPE space. Colabeling for HAP with BoneTag 680 RD and antibodies for selected proteins revealed very distinct staining for amyloid beta, vitronectin, and CFH on the outer surface of the HAP spherules (Fig. 2 *I–K*, respectively). Triple labeling with amyloid beta (red), CFH (green), and HAP (magenta) shows that these proteins can bind to the same HAP spherule simultaneously, and in some surface areas, their immunostaining is so near to each other that they show colocalization (yellow) (Fig. 2*L*). Not all HAP spherules are positive for the tested proteins (Fig. 2*K* and Fig. S5), possibly reflecting localized events, such as site-specific secretion or highly localized inflammatory reactions in a single cell. It is also interesting to note that although there is an enrichment of immunolabeling on the HAP surfaces for vitronectin (Fig. 2*G*), this protein also shows a diffuse labeling around the spherules. Given that we used whole-mount immunolabeling in these experiments and that equal antibody penetration into all deposits could not be ascertained, quantification of the proportion of HAP spherules with the different antibodies was not feasible. Importantly, HAP spherules are present in some cases where no discernable protein deposit is present (as assessed by autofluorescence; Fig. 1 *G* and *H*), suggesting that HAP spherule formation may precede protein build-up and the consequent formation of this component of sub-RPE deposits. Moreover, the spherules described here differ overtly from the 100-nm matrix vesicles implicated in bone formation, which have distinct crystals of HAP enclosed within a lipid shell (34). It is also important to note that immunostaining for several sub-RPE deposit-associated proteins did not show a spherular staining pattern (35); therefore, it appears that there is a selectivity of protein binding to HAP.

To elucidate further the selective binding of proteins to HAP, ARPE-19 cells (a widely used cell model for RPE studies) were grown in a stable, isotope-labeled, amino acid-containing culture medium. Secreted proteins were bound to externally added magnetic HAP-coated beads; the same beads without HAP coating were used as controls. Bound proteins were identified by quantitative MS-based proteomic analysis. The proteins in this complex mixture exhibited selective binding to HAP (Table S2) that included previously identified sub-RPE deposit-associated proteins (labeled red in Table S2): alpha crystalline B (*CRYAB*), amyloid-like protein 2 (*APLP2*), GAPDH, histone H2A.x (*H2AFX*), proteasome subunit beta type 6 (*PSMB6*), and vimentin (*VIM*). This experiment was not designed to replicate the exact conditions in the aging retina in vivo, particularly because we did not culture cells until they were well differentiated and Bruch's membrane and choroid were not present. Therefore, we did not expect to identify all sub-RPE–associated proteins in this mixture because many would be secreted in very small quantities from "unchallenged" RPE cells. Furthermore, many of the sub-RPE deposit-associated proteins originate from blood (7). This experiment was designed to show that proteins have different affinities to HAP and that several proteins actually do not bind to the HAP surface under these conditions (Table S2). Evidently, HAP can provide a surface for preferential binding, and hence concentration of proteins, forming a scaffold for more extensive and less specific binding of proteins, and can lead to sub-RPE deposit growth.

Based on these observations, we propose a novel mechanism for the growth, and perhaps the initiation, of sub-RPE deposits with implications for the development of AMD, which is depicted in Fig. 3. Sub-RPE deposit growth, and maybe even formation, may be mediated, at least partly, by the formation of HAP shells on cholesterol-containing, naturally present extracellular lipid droplets at the RPE/choroid interface (Fig. 3). This calcification process in drusen can be distinguished from the calcification process in atherosclerotic plaques (36, 37), where, instead of extracellular lipid droplets, HAP is deposited on large cholesterol crystals. Whether the HAP deposition in the two diseases shares similarities has yet to be determined, but it is interesting to note that there were suggestions that the two diseases might be related to each other (38). Furthermore, the micrometer-sized extracellular lipid droplets in the core of the HAP spherules in sub-RPE deposits are likely to differ from the smaller (<200 nm) lipoprotein particles described by Curcio et al. (11); therefore, HAP spherule formation underneath the RPE appears to be a novel phenomenon. Once the HAP-coated spherules are formed, they have the capacity to bind different proteins and so provide nucleation sites for the growth of sub-RPE deposits by promoting further protein binding and lipid deposition and entrapment, leading to a self-driven oligomerization process and the growth of sub-RPE deposits to a clinically relevant size (Fig. 3).

Mild to moderate calcification of the elastic layer of Bruch's membrane is commonly observed in aging eyes (20) and can be a sign of accelerated aging (19). Needle-like calcifications, presumed but not proven to be HAP, were described in Bruch's membrane in pseudoxanthoma elasticum (39); however, these calcifications differ from the HAP spherules in location and morphology (Fig. S6). Classic freeze-fracture and scanning electron micrographs show calcium- and phosphorus-containing

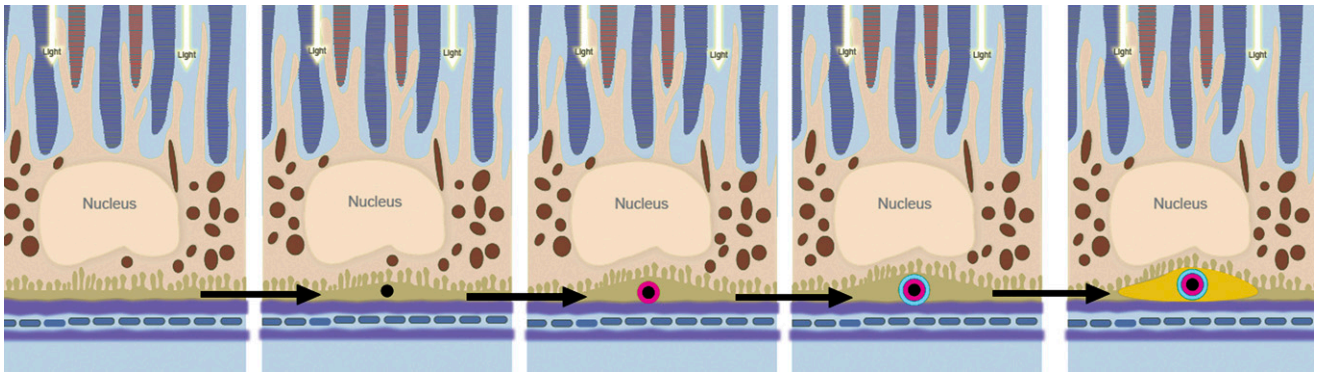

Fig. 3. Simplified diagram of the proposed mechanism for the growth of sub-RPE deposits. Deposit growth is associated with, and perhaps even initiated by, the precipitation of HAP (magenta) onto the naturally present, micrometer-sized, cholesterol-containing extracellular lipid droplets (black). Consequently, different proteins (blue) bind to the HAP surface, which facilitates further deposition in a self-driven oligomerization process, leading ultimately to the formation of the macroscopic sub-RPE deposits (yellow). Melanocytes are depicted as brown particles in the RPE.

spherules similar in size to those spherules shown in this study (40), but these observations have generally been interpreted as dibasic calcium phosphate and not as HAP, and it was not associated with the binding of proteins and the entrapment of lipids. Therefore, HAP spherule formation on the surface of lipid droplets in the inner aspect of Bruch's membrane is a newly recognized phenomenon that differs from previously described calcifications. HAP need not form as a result of a "maturing" process from previously deposited amorphous calcium phosphate: HAP can be directly formed in physiological concentrations of calcium and phosphate at physiological pH (41), and this process may occur in the sub-RPE space. We note that HAP is much harder and less soluble than dibasic calcium phosphate, with the former only being resolubilized by acid secretions in bone remodeling (42). Interestingly, calcified drusen are usually associated with end-stage AMD [especially geographic atrophy (GA)] (43). It is known that drusen resolve as GA develops, and it is possible that the calcific material represents HAP spherules that are resistant to clearing during this process. Sub-RPE deposit formation in the macula is the hallmark of AMD, but deposits are also present in the aging eye without recognized AMD, especially in the peripheral retina (18). Based on post mortem grading for AMD (44), we examined several eyes with sub-RPE deposits in the macula, and all of these eyes contained numerous HAP spherules. However, a precise correlation with the clinical characterization of drusen, such as hard and soft, could not be ascertained by examination of nonfixed samples. Therefore, understanding how the HAP shells form on the ubiquitous cholesterol-containing droplets (9, 10), and how particular proteins bind to these surfaces and initiate the formation of sub-RPE deposits, will be key to improving our understanding of forms of AMD in which this process is important, and may lead to novel early intervention strategies, perhaps before sight-threatening conditions develop.

Methods

HAP Fluorescent Labeling and Immunohistochemistry of Deposit Proteins. Thirty human eyes of donors aged between 43 and 96 y were obtained from the Moorfields Eye Hospital Eye Depository and were phenotyped post mortem based on the Alabama Age-Related Macular Degeneration Grading System for post mortem tissues (44). Samples were obtained within 24 h of death. Full local research ethics committee approval (Moorfields Biobank reference number: 10/H0106/57-2011ETR17) and appropriate consent were obtained in each case. The protocol of the study adhered to the tenets of the Declaration of Helsinki regarding research involving human tissue. Flat mounts of Bruch's membrane/choroid were prepared, after removal of the neurosensory retina and the RPE cells as described previously (27). It is important to note that none of the samples were fixed for these experiments to avoid postmortem chemical interference. Of these samples, six had extensive sub-RPE deposits resembling soft drusen or basal linear/laminar deposits when examined under white light (Nikon LMZ 1500 stereo microscope); a further 10 had numerous focal deposits (hard drusen) in the macula; and all 30 had manifested peripheral, mainly focal, sub-RPE deposits (in Table S1, * indicates the presence of hard drusen and *** indicates extensive focal and/or large diffuse sub-RPE deposits). Basal linear and laminar deposits could not be differentiated on whole mounts, and given the nature of the experiments and the incompatibilities of methodologies for resampling, unambiguous identification of the subtypes of sub-RPE deposits using EM was not possible (27). In some experiments, fixed, paraffin-embedded samples were obtained from the Pathology Archive at the University College London Institute of Ophthalmology. Based on pathology reports describing the presence of different types of sub-RPE deposits in the macula or at the peripheral retina, suitable eyes were selected and 7-μm sections were stained for HAP.

Flat mounts were stained with 1 mg/mL Alizarin Red S (Sigma–Aldrich; excitation wavelength: 532 nm, emission wavelength: 620 nm), 20 μM BoneTag 680RD (Li-Cor; excitation wavelength: 620 nm, emission wavelength: 680 nm), 1 mg/mL tetracycline (Sigma–Aldrich; excitation wavelength: 405 nm, emission wavelength: 570 nm), or 1 mg/mL Xylenol Orange (Sigma–Aldrich; excitation wavelength: 532 nm, emission wavelength: 570 nm), all in aqueous buffer for 20 min at room temperature. Nile Red (Invitrogen; excitation wavelength: 532 nm, emission wavelength: 620 nm) was first dissolved in acetone and then diluted in aqueous buffer to 3.5 mg/mL, and tissues were incubated for 20 min at room temperature.

Immunohistochemistry was also performed on unfixed, flat-mounted Bruch's membrane/choroid tissue, obtained as above. Flat mounts were blocked with goat serum and then incubated with primary and secondary antibodies for 2 h each at 30 °C. The primary antibodies used were anti-CFH (Santa Cruz Biotechnology; 1/100 dilution), antivitronectin (AbDSerotec; 1/200 dilution), and anti-amyloid β (6E10, Covance; 1/100 dilution). Alexa-Fluor 488 Goat anti-rabbit and Alexa-Fluor 568 Goat anti-rat secondary antibodies were from Invitrogen and used at a 1:1,000 dilution. Samples were imaged using a Zeiss LSM700 confocal microscope through a 63×/1.2 N.A. Zeiss Neofluar objective.

Mapping of Drusen Constituents by TOF-SIMS Imaging. Flat mounts on glass slides were transported and stored at −20 °C, and immediately before analysis, they were placed in a freeze dryer for 4 h to ensure the samples were compatible with the ultrahigh-vacuum conditions of the SIMS instruments. To expose the internal structure of drusen, an FIB milling approach was implemented using an FEI FIB200 secondary ion mass spectrometer. Following gold sputter coating to ensure a conducting surface, the glass slide was mounted on the sample stage. Using an increased ion beam current, the upper 1 μm was removed sequentially until the required region of the drusen was reached (Fig. 2).

For MS imaging at submicron resolution over *m/z* 0–880, the slide was immediately transferred to a TOF-SIMS.5 (ION-TOF) secondary ion mass spectrometer. The system comprises a bismuth primary ion beam, operating at 25 kV and tuned to use the Bi_3^+ cluster for greater secondary ion yield, and a low-energy electron flood gun for charge compensation. Ionic species sputtered from the surface under the bismuth bombardment are steered into a reflectron TOF mass analyzer.

All data analysis and visualization were performed using in-house written MATLAB (MathWorks) functions. Nonnegative matrix factorization was performed on the data to reduce their dimensionality into five chemically distinct factors. Peaks identified as strongly localized to the spherules were identified from the factors, and single ion images were produced (Fig. 2). The overall protein signature was based on summing a combination of characteristic immonium ions; the PC distribution was visualized by the PC headgroup peak at *m/z* 184.07, and cholesterol was visualized by its $[M^+H^-H_2O]^+$ ion at *m/z* 369.38.

μXRD Analysis of Drusen. μXRD analyses of drusen were conducted at beamline X26A (National Synchrotron Light Source, Brookhaven National Laboratory). Tissue samples containing drusen were flat-mounted on 4-μm-thick Ultralene film (Volga Instruments) for analysis. Monochromatic X-rays were used tuned to an incident wavelength of 0.70926 Å, corresponding to 17.481 keV of energy, using a channel-cut Si(111) monochromator crystal. The incident beam was focused to a spot size of 9 (horizontal) × 5 (vertical) μm on the sample using Rh-coated silicon mirrors in a Kirkpatrick–Baez geometry. The X-ray diffraction from the sample was measured using a Rayonix SX165 CCD area detector. Calibrations and corrections for detector distortions (camera – sample distance, camera tilt and rotation, and the beam center on the camera plane) were done using FIT2D software (45) and corrected using a National Institute of Standards and Technology SRM 674a corundum standard and silver behenate. The 2D area detector data were integrated into 2θ-intensity using FIT2D, and HAP was then identified by comparison with reference powder diffraction patterns (International Centre for Diffraction Data, 2003) using Match software (Crystal Impact).

Identification of HAP-Bound Proteins Secreted from Cultured RPE Cells by Stable Isotope Labeling with Amino Acids in Cell Culture.

Cell culture. For stable isotope labeling with amino acids in cell culture (SILAC) experiments, ARPE-19 cells were grown in SILAC DMEM/F12 medium (PAA) supplemented with 10% (vol/vol) dialyzed FBS (PAA); 1% (vol/vol) penicillin-streptomycin; and $^{12}C_6,^{14}N_2$ lysine plus $^{12}C_6,^{14}N_4$ arginine (light medium) or $^{13}C_6$ lysine plus $^{13}C_6,^{15}N_4$ arginine (heavy medium). Proline (0.5 mM) was added to all SILAC media to prevent arginine-to-proline conversion (46). All amino acids were purchased from Silantes. Subconfluent cultures were thoroughly washed with PBS and kept in serum-free medium for 24 h. Label-swap replication was used for enhanced reliability in affinity ratios. Equal amounts of "heavy" supernatants were incubated either with BcMag HAP-coated magnetic silica beads (Bioclone) or with unmodified silica beads (negative control). "Light" supernatants were processed in the same way. After incubating for 3 h on a rotator at 25 °C, bound proteins were washed with serum-free medium (two times for 15 min each time). Finally, the beads were resuspended in 30 μL of 50-mmol/L ammonium bicarbonate and subjected to on-bead tryptic digestion. The

corresponding samples (eluates from light-labeled HAP and heavy-labeled control beads, and vice versa) were mixed as described earlier (47) before being subjected to liquid chromatography tandem MS (LC-MS/MS).

MS and data analysis. LC-MS/MS analysis was performed on an UltiMate 3000 Nano HPLC system (Dionex) coupled to an LTQ OrbitrapXL mass spectrometer (Thermo Fisher Scientific) by a nano-spray ion source. For SILAC experiments, all acquired spectra were processed and analyzed using MaxQuant version 1.3.0.5 (www.maxquant.org/) and the human-specific UniProt (www.maxquant.org/) in combination with Mascot (version 2.2; Matrix Science). Cysteine carbamidomethylation was selected as a fixed modification; methionine oxidation and protein acetylation were allowed as variable modifications. The peptide and protein false discovery rates were set to 1%. Contaminants like keratins were removed. Proteins identified and quantified by at least two peptides per experiment were considered for further analysis. Each experiment consisted of a forward labeling approach and a reverse labeling approach (label swapping) to exclude label-specific effects. A *P* value of 0.001 was selected as the threshold for significant enrichment or alteration.

ACKNOWLEDGMENTS. We thank Profs. Philip J. Luthert, Jonathan Knowles, and Frederik Van Kuijk for their help and advice; Lajos Csincsik and Robert Tripon for technical assistance; and Krystyna Grycynska and Anne Thompson for some of the drawings. The research was supported by the Bill Brown Charitable Trust Senior Research Fellowship, Moorfields Eye Hospital Special Trustees, and Mercer Fund from Fight for Sight (to I.L.) and by a grant from Bright Focus Foundation (to R.B.T. and I.L.). The TOF-SIMS analysis was funded by the Engineering and Physical Sciences Research Council, United Kingdom (Grant EP/H006060/1) and by the Natural Environment Research Council, United Kingdom (Grant NE/J013382/1). Portions of this work were performed at Beamline X26A [National Synchrotron Light Source (NSLS), Brookhaven National Laboratory] under a general user grant (to J.M.F.). Beamline X26A is supported, in part, by the US Department of Energy (DOE) Geosciences (Grant DE-FG02-92ER14244) to The University of Chicago (Centre for Advanced Radiation Sources). Use of the NSLS was supported by the DOE, Office of Science, Office of Basic Energy Sciences, under Contract DE-AC02-98CH10886. Tissue for this project was provided by the University College London Institute of Ophthalmology and Moorfields Eye Hospital Eye Tissue Repository supported by National Institute for Health Research funding.

1. Crabb JW, et al. (2002) Drusen proteome analysis: An approach to the etiology of age-related macular degeneration. *Proc Natl Acad Sci USA* 99(23):14682–14687.
2. Pauleikhoff D, Harper CA, Marshall J, Bird AC (1990) Aging changes in Bruch's membrane. A histochemical and morphologic study. *Ophthalmology* 97(2):171–178.
3. Sarks SH (1976) Ageing and degeneration in the macular region: A clinico-pathological study. *Br J Ophthalmol* 60(5):324–341.
4. Bird AC (2010) Therapeutic targets in age-related macular disease. *J Clin Invest* 120(9): 3033–3041.
5. Moore DJ, Hussain AA, Marshall J (1995) Age-related variation in the hydraulic conductivity of Bruch's membrane. *Invest Ophthalmol Vis Sci* 36(7):1290–1297.
6. Bird AC, Phillips RL, Hageman GS (2014) Geographic atrophy: A histopathological assessment. *JAMA Ophthalmol* 132(3):338–345.
7. Johnson LV, et al. (2011) Cell culture model that mimics drusen formation and triggers complement activation associated with age-related macular degeneration. *Proc Natl Acad Sci USA* 108(45):18277–18282.
8. Kunchithapautham K, Atkinson C, Rohrer B (2014) Smoke exposure causes endoplasmic reticulum stress and lipid accumulation in retinal pigment epithelium through oxidative stress and complement activation. *J Biol Chem* 289(21):14534–14546.
9. Rudolf M, Seckerdieck K, Grisanti S, Curcio CA (2014) Internal structure consistent with remodelling in very small drusen, revealed by filipin histochemistry for esterified cholesterol. *Br J Ophthalmol* 98(5):698–702.
10. Curcio CA, Johnson M, Rudolf M, Huang JD (2011) The oil spill in ageing Bruch membrane. *Br J Ophthalmol* 95(12):1638–1645.
11. Curcio CA, Johnson M, Huang JD, Rudolf M (2010) Apolipoprotein B-containing lipoproteins in retinal aging and age-related macular degeneration. *J Lipid Res* 51(3): 451–467.
12. Rudolf M, Curcio CA (2009) Esterified cholesterol is highly localized to Bruch's membrane, as revealed by lipid histochemistry in wholemounts of human choroid. *J Histochem Cytochem* 57(8):731–739.
13. Curcio CA, Johnson M, Huang JD, Rudolf M (2009) Aging, age-related macular degeneration, and the response-to-retention of apolipoprotein B-containing lipoproteins. *Prog Retin Eye Res* 28(6):393–422.
14. Miller JW (2013) Age-related macular degeneration revisited—Piecing the puzzle: The LXIX Edward Jackson memorial lecture. *Am J Ophthalmol* 155(1):1–35.e13.
15. Luibl V, et al. (2006) Drusen deposits associated with aging and age-related macular degeneration contain nonfibrillar amyloid oligomers. *J Clin Invest* 116(2):378–385.
16. Russell SR, Mullins RF, Schneider BL, Hageman GS (2000) Location, substructure, and composition of basal laminar drusen compared with drusen associated with aging and age-related macular degeneration. *Am J Ophthalmol* 129(2):205–214.
17. Lengyel I, et al. (2007) High concentration of zinc in sub-retinal pigment epithelial deposits. *Exp Eye Res* 84(4):772–780.
18. Flinn JM, Kakalec P, Tappero R, Jones B, Lengyel I (2014) Correlations in distribution and concentration of calcium, copper and iron with zinc in isolated extracellular deposits associated with age-related macular degeneration. *Metallomics* 6(7):1223–1228.
19. Davis WL, Jones RG, Hagler HK (1981) An electron microscopic histochemical and analytical X-ray microprobe study of calcification in Bruch's membrane from human eyes. *J Histochem Cytochem* 29(5):601–608.
20. Vogt SD, et al. (2011) Retinal pigment epithelial expression of complement regulator CD46 is altered early in the course of geographic atrophy. *Exp Eye Res* 93(4):413–423.
21. Raggatt LJ, Partridge NC (2010) Cellular and molecular mechanisms of bone remodeling. *J Biol Chem* 285(33):25103–25108.
22. van der Schaft TL, de Bruijn WC, Mooy CM, Ketelaars DA, de Jong PT (1992) Element analysis of the early stages of age-related macular degeneration. *Arch Ophthalmol* 110(3):389–394.
23. Skinner HC, Nalbandian J (1975) Tetracyclines and mineralized tissues: Review and perspectives. *Yale J Biol Med* 48(5):377–397.
24. Kovar JL, et al. (2011) Near-infrared-labeled tetracycline derivative is an effective marker of bone deposition in mice. *Anal Biochem* 416(2):167–173.
25. Vilmann H (1969) The in vivo staining of bone with alizarin red S. *J Anat* 105(Pt 3): 533–545.
26. Rahn BA, Perren SM (1971) Xylenol orange, a fluorochrome useful in polychrome sequential labeling of calcifying tissues. *Stain Technol* 46(3):125–129.
27. Lengyel I, et al. (2004) Association of drusen deposition with choroidal intercapillary pillars in the aging human eye. *Invest Ophthalmol Vis Sci* 45(9):2886–2892.
28. Raggio CL, Boyan BD, Boskey AL (1986) In vivo hydroxyapatite formation induced by lipids. *J Bone Miner Res* 1(5):409–415.
29. Fletcher JS, Vickerman JC (2013) Secondary ion mass spectrometry: Characterizing complex samples in two and three dimensions. *Anal Chem* 85(2):610–639.
30. Wang L, et al. (2010) Abundant lipid and protein components of drusen. *PLoS ONE* 5(4):e10329.
31. Hageman GS, et al. (2005) A common haplotype in the complement regulatory gene factor H (HF1/CFH) predisposes individuals to age-related macular degeneration. *Proc Natl Acad Sci USA* 102(20):7227–7232.
32. Hageman GS, Mullins RF, Russell SR, Johnson LV, Anderson DH (1999) Vitronectin is a constituent of ocular drusen and the vitronectin gene is expressed in human retinal pigmented epithelial cells. *FASEB J* 13(3):477–484.
33. Cummings LJ, Snyder MA, Brisack K (2009) Protein chromatography on hydroxyapatite columns. *Methods Enzymol* 463:387–404.
34. Anderson HC, Garimella R, Tague SE (2005) The role of matrix vesicles in growth plate development and biomineralization. *Front Biosci* 10:822–837.
35. Mullins RF, Russell SR, Anderson DH, Hageman GS (2000) Drusen associated with aging and age-related macular degeneration contain proteins common to extracellular deposits associated with atherosclerosis, elastosis, amyloidosis, and dense deposit disease. *FASEB J* 14(7):835–846.
36. Laird DF, Mucalo MR, Yokogawa Y (2006) Growth of calcium hydroxyapatite (Ca-HAp) on cholesterol and cholestanol crystals from a simulated body fluid: A possible insight into the pathological calcifications associated with atherosclerosis. *J Colloid Interface Sci* 295(2):348–363.
37. Bertazzo S, et al. (2013) Nano-analytical electron microscopy reveals fundamental insights into human cardiovascular tissue calcification. *Nat Mater* 12(6):576–583.
38. Vingerling JR, et al. (1995) The prevalence of age-related maculopathy in the Rotterdam Study. *Ophthalmology* 102(2):205–210.
39. Jensen OA (1977) Bruch's membrane in pseudoxanthoma elasticum. Histochemical, ultrastructural, and x-ray microanalytical study of the membrane and angioid streak areas. *Albrecht Von Graefes Arch Klin Exp Ophthalmol* 203(3-4):311–320.
40. Ulshafer RJ, Allen CB, Nicolaissen B, Jr, Rubin ML (1987) Scanning electron microscopy of human drusen. *Invest Ophthalmol Vis Sci* 28(4):683–689.
41. Boskey AL, Posner AS (1976) Formation of hydroxyapatite at low supersaturation. *J Phys Chem* 80(1):40–45.
42. Rudolf M, et al. (2008) Prevalence and morphology of druse types in the macula and periphery of eyes with age-related maculopathy. *Invest Ophthalmol Vis Sci* 49(3): 1200–1209.
43. Panorgias A, et al. (2013) Multimodal assessment of microscopic morphology and retinal function in patients with geographic atrophy. *Invest Ophthalmol Vis Sci* 54(6): 4372–4384.
44. Curcio CA, Medeiros NE, Millican CL (1998) The Alabama Age-Related Macular Degeneration Grading System for donor eyes. *Invest Ophthalmol Vis Sci* 39(7):1085–1096.
45. Hammersley AP (1998) FIT2D V9.129 Reference Manual V3.1. *ESRF Internal Report*, ESRF98HA01T.
46. Bendall SC, et al. (2008) Prevention of amino acid conversion in SILAC experiments with embryonic stem cells. *Mol Cell Proteomics* 7(9):1587–1597.
47. Gloeckner CJ, Boldt K, Ueffing M (2009) Strep/FLAG tandem affinity purification (SF-TAP) to study protein interactions. *Curr Protoc Protein Sci*, Chap 19:Unit 19.20.